

Process Design and Optimization for the Continuous Manufacturing of Nevirapine, an Active Pharmaceutical Ingredient for HIV Treatment

Samir Diab,[†] D. Tyler McQuade,[‡] B. Frank Gupton,[‡] and Dimitrios I. Gerogiorgis^{*,†} 

[†]Institute for Materials and Processes (IMP), School of Engineering, University of Edinburgh, The Kings Buildings, Edinburgh EH9 3FB, Scotland, U.K.

[‡]Department of Chemical and Life Sciences Engineering, School of Engineering, Virginia Commonwealth University, Richmond, Virginia 23284-3028, United States

ABSTRACT: The development of efficient and cost-effective manufacturing routes toward HIV active pharmaceutical ingredients (APIs) is essential to ensure their global and affordable access. Continuous pharmaceutical manufacturing (CPM) is a new production paradigm for the pharmaceutical industry whose potential for enhanced efficiency and economic viability over currently implemented batch protocols offers promise for improving HIV API production. Nevirapine is a widely prescribed HIV API whose continuous flow synthesis was recently demonstrated. This paper presents the technoeconomic optimization of nevirapine CPM, including the continuous flow synthesis and a conceptual continuous crystallization. Arrhenius law parameter estimation from published reaction kinetic data allows explicit modeling of the temperature dependence of the reaction performance, and an experimentally validated aqueous API solubility computation method is used to model crystallization processes. A nonlinear optimization problem for cost minimization is formulated for comparative evaluation of different plant designs. Higher reactor temperatures are favored for CPM total cost minimization, while lower pH (less neutralizing agent) is required to attain the desired plant capacities for cost-optimal configurations compared with batch crystallization designs. Suitable E-factors for pharmaceutical manufacturing are attained when higher solvent recoveries are assumed. Implementing CPM designs significantly lowers the nevirapine cost of goods toward reducing the price of societally important HIV medicines.

1. INTRODUCTION

Affordability and accessibility of essential medicines remain pressing issues for the treatment of diseases prevalent in developing countries. Treatment of the human immunodeficiency virus (HIV) continues to be one of the most prominent global health challenges; the prevalence of the virus has been historically increasing worldwide, with low- and middle-income countries being most affected (Figure 1). The development of efficient, cost-effective manufacturing routes toward drugs for HIV treatment is paramount to ensure global, affordable access to such medicines.¹

Continuous pharmaceutical manufacturing (CPM) has emerged as a new production paradigm because of its promise of enhanced efficiency and greater economic viability over currently implemented batch protocols.^{4,5} The utility of CPM platforms for the development of active pharmaceutical ingredients (APIs) for the treatment of HIV and other societally important diseases has been demonstrated in the literature;^{6,7} Table 1 lists various HIV APIs whose syntheses have benefited by the implementation of semicontinuous/continuous flow methods. While experimental demonstration of feasible API continuous synthetic routes is the foundation of any CPM campaign,^{7,8} the design of continuous separation processes for integration into upstream CPM is essential to realize the benefits of end-to-end continuous manufacturing for HIV API production.⁹

Nevirapine is a widely prescribed API for HIV-1 treatment on the World Health Organization (WHO) List of Essential Medicines, whose continuous flow synthesis from two

advanced starting materials was recently demonstrated with subsequent purification and batch crystallization for final API separation.¹⁰ Additionally, various routes toward one of the API synthesis starting materials, 2-chloro-3-amino-4-picoline (CAPIC), have also been presented in the literature.^{11,12} The economic viability of different process alternatives for the API has not yet been systematically investigated and is essential to ensure cost-optimal designs. Systematic comparison of process alternatives is essential to further aid the development of leaner manufacturing routes for nevirapine.¹³

Modeling and optimization methodologies can be used to establish optimal process design configurations.^{13,14} Advanced theoretical methods have been previously implemented toward optimal pharmaceutical unit design¹⁵ and optimization of pharmaceutical manufacturing processes to elucidate optimal operation, analysis of synthetic pathways,^{16–18} and life cycle assessments.^{19,20} Modeling and optimization have also been implemented in the design of separation processes in pharmaceutical manufacturing, such as liquid–liquid extraction (LLE),^{21–23} crystallization,^{24–30} and chromatographic methods.³¹ Identification of cost-optimal plantwide designs is essential,¹⁵ particularly end-to-end designs encompassing synthesis and purification/separation. Elucidating cost-optimal designs for nevirapine CPM will further aid process development for this societally important API.^{5,32}

Received: November 17, 2018

Published: January 4, 2019

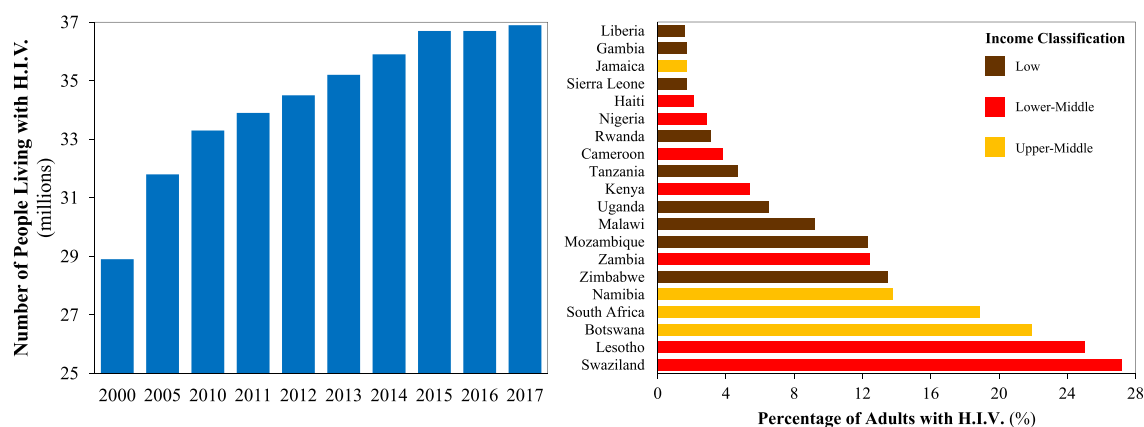


Figure 1. Increasing worldwide HIV prevalence² and the top 20 countries with the highest viral rates.³

Table 1. Demonstrated Continuous/Semicontinuous Flow Syntheses of HIV APIs.

API	year	type	processing benefits	ref
efavirenz	2013	semicontinuous	improved API yield reduced process time reduced number of unit operations	33
darunavir	2015	continuous	end-to-end continuous process at production scale	34, 35
lamivudine	2017	semicontinuous	improved API yield reduced process time	36
nevirapine	2017	continuous	improved material efficiency reduced number of unit operations	10
dolutegravir	2018	continuous	reduced process time	37

This work conducts a systematic comparative evaluation of CPM process alternatives for nevirapine based upon the published synthetic routes via steady-state process modeling and optimization.^{10–12} The continuous processes for nevirapine demonstrated in the literature are first presented. A conceptual continuous crystallization process is considered for comparison to the demonstrated batch crystallization process. Arrhenius parameter estimation from experimental kinetic data allows the design of a flow reactor for the continuous synthesis of nevirapine. Crystallization process design utilizes an established API solubility model.³⁸ Costing methodologies for pharmaceutical process alternatives are presented.⁵ A constrained nonlinear optimization problem for total cost minimization of different design alternatives is then formulated. Optimal total cost components, plant material efficiencies, and corresponding operating parameters are presented for different process configurations for comparative evaluation to establish the most promising designs for nevirapine production.

2. PROCESS MODELING, SIMULATION, AND OPTIMIZATION

2.1. API and Starting Material Synthetic Routes.

Various commercial routes toward nevirapine have been demonstrated in the literature with varying complexities and

material intensities.³⁹ The recent demonstration of the continuous flow synthesis of nevirapine uses the advanced starting materials CAPIC and methyl 2-(cyclopropylamino)-nicotinate (MeCAN).¹⁰ The syntheses of CAPIC and MeCAN are summarized in Figure 2.

Figure 2a presents the published batchwise synthesis of CAPIC. Acetone and malononitrile (**2**) react in toluene (PhMe) in the presence of basic Al_2O_3 at 15–20 °C to form ylidene **3**, followed by filtration of Al_2O_3 from the reaction mixture. Dimethylformamide–dimethyl sulfate (DMF–DMS, **4**), acetic anhydride (Ac_2O), and triethylamine (TEA) are then added to the filtrate under N_2 to form enamine **5**. Hydrogen chloride (HCl) gas is then bubbled into the reaction mixture, followed by heating to 50 °C. The mixture is then concentrated by evaporation of the solvent and water followed by filtration of the product, 2-chloro-4-methylnicotinonitrile (CYCIC, **6**). Sulfuric acid (H_2SO_4) is then added to the solid CYCIC, and the mixture is reacted at high temperature, followed by the addition of water. An aqueous solution of NaOH is added at 40 °C until the pH reaches 11. The resulting suspension is then filtered to obtain the product, 2-chloro-4-methylnicotinamide (COMAD, **7**). A mixture of COMAD, water, and sodium hypobromite (NaOBr) is made at 0 °C. Water is then added, and the mixture is heated to 80 °C, stirred, and cooled to 50 °C. Toluene (PhMe) is added to form a biphasic mixture; the organic layer is washed with water and concentrated under vacuum to remove the solvent. Hexanes are then added to precipitate CAPIC.

Figure 2b shows the published batchwise synthesis of MeCAN. 2-Chloronicotinonitrile (**9**), cyclopropylamine (CPA), TEA, water, and isopropyl alcohol (IPA) are added at 140 °C and pressurized to 10 psi to form intermediate **10**. The mixture is stirred and then cooled to 60 °C. Potassium hydroxide (KOH) is added to the reaction mixture, which is then stirred. Concentrated HCl is added to change the pH to 6, and the mixture is cooled to 10 °C to precipitate 2-(cyclopropylamino)nicotinic acid (2-CAN, **11**), which is then vacuum-filtered. 2-CAN is then dissolved in PhMe under N_2 , and thionyl chloride (SOCl_2) is added. The reaction mixture is cooled to 0 °C, followed by H_2O addition and adjustment of the pH to 9 with aqueous NaOH solution, and a biphasic mixture forms. The aqueous layer is washed with PhMe, and the combined organic layers are washed with H_2O , dried with Mg_2SO_4 , filtered, and concentrated under vacuum to yield MeCAN.

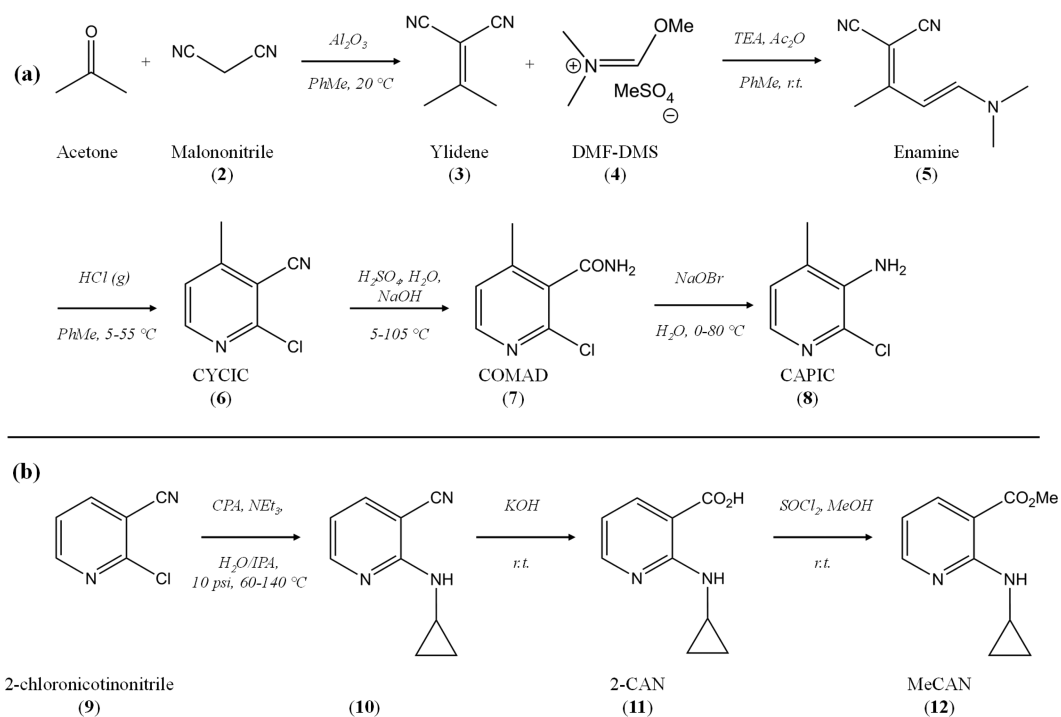


Figure 2. Published batchwise syntheses of (a) CAPIC and (b) MeCAN.¹⁰

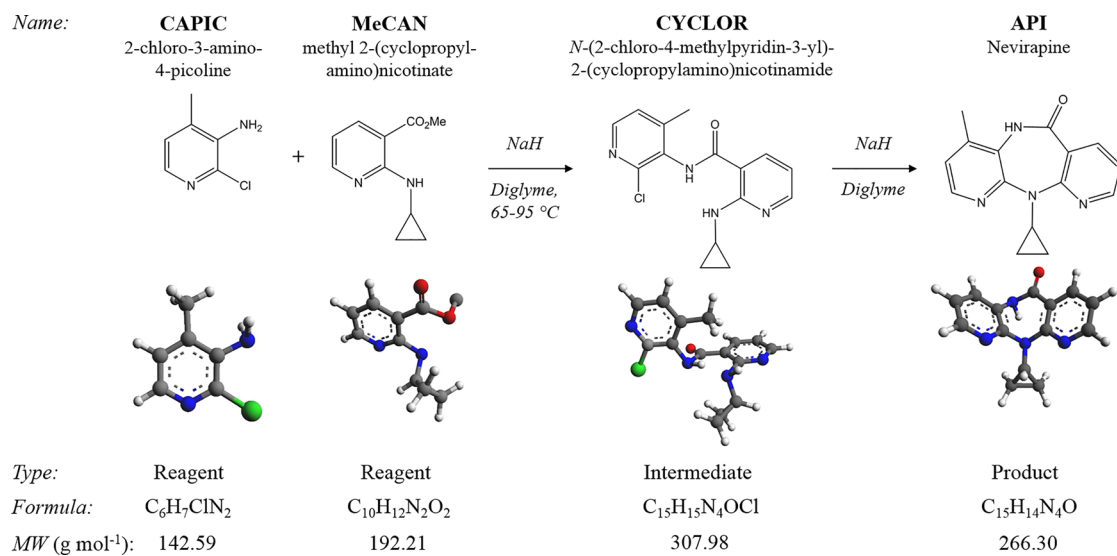


Figure 3. Continuous synthetic strategy to obtain nevirapine from CAPIC and MeCAN.¹⁰

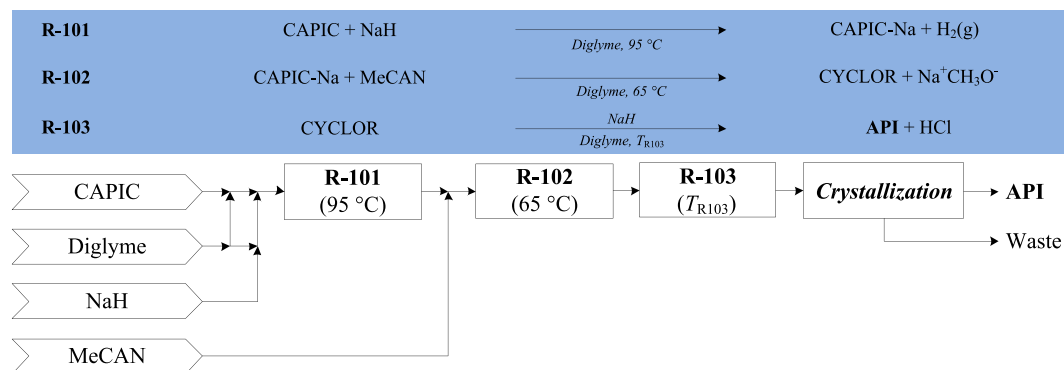


Figure 4. Process flowsheet for the CPM of nevirapine.

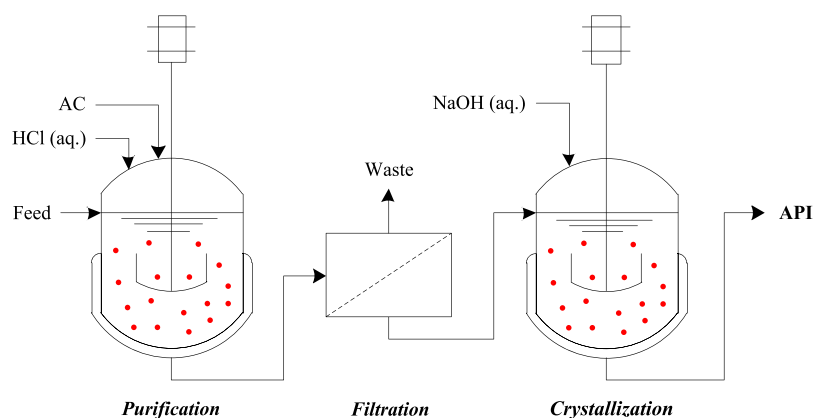


Figure 5. Crystallization of the API operated in batch (BX) or continuous (CPM) mode.¹⁰

Table 2. Summary of Continuous Flow Reactor Conditions Used in Process Modeling

reactor	reaction	T (°C)	τ	X_A (%)
R-101	CAPIC + NaH \rightarrow CAPIC-Na	95	8.56 s	100
R-102	CAPIC-Na + MeCAN \rightarrow CYCLOR	65	2 h	82.5
R-103	CYCLOR \rightarrow API	variable	21 min	$X_A^{R103} = f(T_{R103})$

The published continuous synthetic route from CAPIC and MeCAN is shown in Figure 3.¹⁰ The starting materials CAPIC and MeCAN (in diglyme carrier solvent) are used to form the intermediate *N*-(2-chloro-4-methylpyridin-3-yl)-2-(cyclopropylamino)nicotinamide (CYCLOR) in the presence of NaH, which then forms nevirapine (the API). The CPM process in this work is based upon this demonstrated continuous flow synthesis, whose process modeling and simulation are further developed in later subsections.

2.2. Process Flowsheets. Figure 4 shows the process flowsheet for nevirapine CPM based on the published continuous flow synthesis.¹⁰ The first reactor, R-101, is a thin-film reactor operated at 95 °C; reaction between CAPIC (3 M) and NaH (2 M) in diglyme at 95 °C forms the sodium salt of CAPIC (CAPIC-Na) with evolution of H₂ gas and an estimated 100% conversion of CAPIC. The mixture containing CAPIC-Na is added to a stirred tank (R-102, 65 °C) with neat MeCAN (1.05 equiv), giving a reported 82.5% conversion of CAPIC-Na to CYCLOR (plus sodium methoxide, NaCH₃O). Finally, CYCLOR undergoes ring closure in the presence of a packed bed of NaH (R-103) to form the API. Various reaction performances at different temperatures (T_{R103}) are reported in the demonstrated continuous flow synthesis,¹⁰ as discussed further in section 2.3.1.3.

The flowsheet for the crystallization process following the continuous flow synthesis is shown in Figure 5. The effluent of R-103 is fed to a stirred tank where aqueous HCl is added; the API is more soluble at lower pH in aqueous solutions. Activated carbon (AC) is also added to adsorb organic impurities prior to their subsequent removal via filtration.¹⁰ Nevirapine is then crystallized from the solution by decreasing its solubility by increasing the pH by addition of aqueous NaOH solution. The crystallization following the continuous flow synthesis can be implemented in either batch (BX) or continuous (CPM) mode. Details of crystallization modeling are provided in section 2.3.2.

2.3. Modeling and Nonlinear Optimization. **2.3.1. Reactor Design and Kinetic Parameter Estimation.** Plantwide mass balances are required for detailed unit operation

modeling and plantwide performance analysis. Molar balances across each reactor are calculated via eq 1.

$$F_i^j = F_{A,0}^j(\Theta_i^j + \nu_i^j X_A^j) \quad (1)$$

where F_i^j is the molar flow rate of component i exiting reactor j , $F_{A,0}^j$ is the inlet molar flow rate of limiting reagent A in reactor j , Θ_i^j is the molar ratio of component i to limiting reagent A in reactor j , ν_i^j is the stoichiometric coefficient of component i in reactor j , and X_A^j is the conversion of limiting reagent A in reactor j . The modeling and design of each reactor in the process flowsheet (Figure 4) are now discussed. The fixed process conditions required for each of the three reactors are summarized in Table 2.

2.3.1.1. Reactor R-101. Full conversion of CAPIC (limiting reagent) to CAPIC-Na ($X_A^{R101} = 100\%$) is reported for an R-101 operating temperature (T_{R101}) of 95 °C and an estimated residence time (τ) of 8.56 s; this stoichiometric conversion in a short residence time is allowed by implementation of a thin-film reactor to enhance and heat and mass transfer to expedite the reaction.¹⁰ The operating temperature of R-101 is chosen to be the same as in the published experimental demonstration ($T_{R101} = 95$ °C); thus, the same reaction performance ($X_A^{R101} = 100\%$) is assumed for modeling of CAPIC-Na formation.

2.3.1.2. Reactor R-102. A conversion of CAPIC-Na (limiting reagent) to CYCLOR of 82.5% is reported for $T_{R102} = 65$ °C and $\tau = 2$ h.¹⁰ The operating temperature of R-102 is chosen to be the same as in the published experimental demonstration ($T_{R102} = 65$ °C); thus, the same reaction performance ($X_A^{R102} = 82.5\%$) and residence time ($\tau = 2$ h) are assumed for modeling of CYCLOR formation.

2.3.1.3. Reactor R-103. Temperature-dependent kinetic data for API formation in R-103 are available in the literature;¹⁰ at temperatures of 120, 140 and 165 °C, CYCLOR conversions to API of 10, 60, and 96% are attainable, respectively, each for an estimated residence time of 21 min.¹⁰ The packed bed reactor (PBR) design equation is provided in eq 2:

$$\tau_{R103} = C_{A,0} \int_0^{X_A} \frac{dX_A}{-r_A} \quad (2)$$

where τ_{R103} is the residence time of R-103, $C_{A,0}$ is the concentration of the limiting reagent (CYCLOR), and r_A is the rate of reaction of the limiting reagent. CYCLOR is the limiting reagent because NaH in the packed bed is in significant excess, so it is assumed that the reaction is first-order in CYCLOR. Following this assumption, the first-order rate constants, k , at different temperatures can be estimated. This allows regression of the Arrhenius law (eq 3) parameters (the pre-exponential factor, A , and activation energy, E_a) for API formation, allowing explicit modeling of CYCLOR conversion to the API as a function of temperature, T :

$$k(T) = A \exp\left(-\frac{E_a}{RT}\right) \quad (3)$$

where R is the universal gas constant. The Arrhenius plot from the available kinetic data is shown in Figure 6 with a good fit

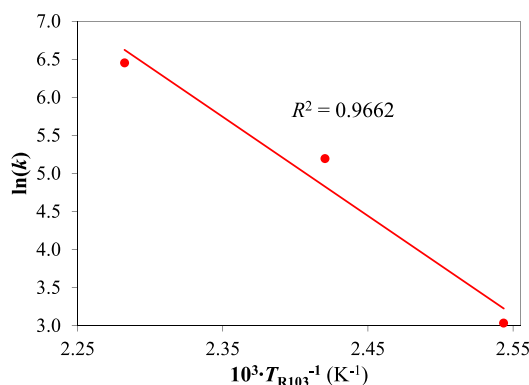


Figure 6. Arrhenius plot for ring closure of CYCLOR to API in the continuous flow synthesis.

(coefficient of determination $R^2 > 0.96$); the regressed parameters are $E_a = 1.565 \text{ kJ mol}^{-1}$ and $A = 8.49 \times 10^{13} \text{ s}^{-1}$, assuming that R-103 is first-order in CYCLOR. The availability of a wider kinetic data set will allow further validation of Arrhenius parameter estimation results and investigation of more complex candidate rate law expressions.

2.3.2. Crystallization Process. The batch crystallization has a reported yield of 96% in a residence time of 1 h operating at 25 °C and a crystallisation pH, $\text{pH}_{\text{CRYST}} = 7$.¹⁰ Here we compare the conceptual steady-state continuous crystallization to the demonstrated batch process by varying the pH of the continuous crystallization. Table 3 summarizes the fixed processing conditions for the batch and continuous crystallization process designs.

Table 3. Summary of Fixed Process Conditions for the Batch and Continuous Crystallization Process Models

	BX	CPM
temperature (°C)	25	25
thermodynamic efficiency (%)	100	70
τ (h)	1	0.5
feed pH	~0.5	~0.5
operating pH, pH_{CRYST}	7	variable
yield, Y (%)	96	$Y = f(\text{pH}_{\text{CRYST}})$

Crystallization process design requires modeling of the API solubility in process mixtures. The mixture prior to the pH increase for API crystallization is predominantly aqueous (solvent H_2O content > 96 mol %), and thus, the mixture is assumed to be purely aqueous for crystallization modeling purposes. The aqueous solubility, S , of nevirapine in the crystallization stage (see Figure 5) as a function of pH is modeled by³⁸

$$S = S_0(1 + 10^{\text{p}K_a - \text{pH}}) \quad (4)$$

where $S_0 = 4.58 \times 10^{-2} \text{ g L}^{-1}$ is the solubility under nonionizing conditions and $\text{p}K_a = 2.8$ at 25 °C;³⁸ correlation parameter values (S_0 and $\text{p}K_a$) are available only at 25 °C, and thus, additional temperatures for cooling crystallization modeling cannot be considered. Figure 7 shows the modeled

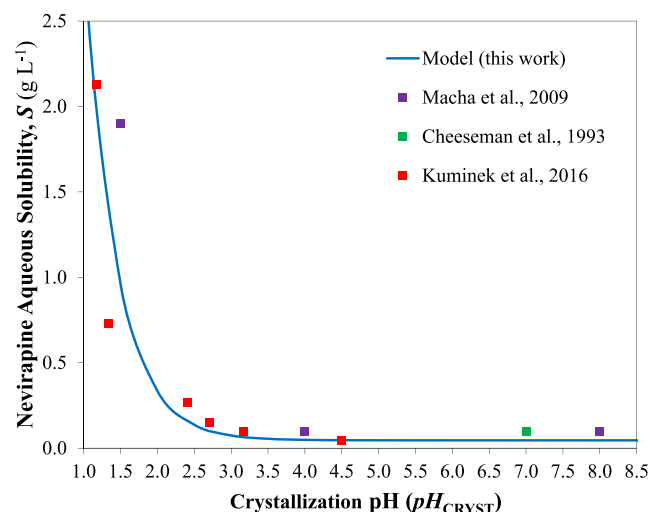


Figure 7. Comparison of the aqueous API solubility model, $S = f(\text{pH})$, with experimental values.^{38,40,41}

aqueous API solubility as a function of pH with experimental values as reported by various literature references.^{38,40,41} The model shows good agreement with the experimental values.

The crystallization yield is estimated from the API concentration in the mother liquor, C_{CRYST} , and the aqueous API solubility, S , according to eq 5:

$$Y = 1 - \frac{C_{\text{CRYST}}}{S} \quad (5)$$

The feed streams for both the batch and continuous crystallization processes enter at $\text{pH} \approx 0.5$. A residence time of 0.5 h is assumed for the continuous crystallization; this value is lower than that for the batch crystallization (1 h) to reflect the difference in residence times typical of these different operation modes. It is assumed that the batch crystallization attains full (100%) thermodynamic equilibrium. A conservative thermodynamic efficiency of 70% is assumed for the continuous crystallization to account for uncertainty in the assumed residence time and the calculated yield. This will likely result in an underprediction of the continuous crystallization yield and thus an overestimation of total costs, which should be considered when interpreting the optimization results presented here. The use of detailed crystallization kinetics data for nevirapine as well as dynamic and steady-state crystallization models for the batch and continuous crystallization processes, respectively, will provide more detailed

Table 4. Parameters for Scaled Equipment Purchase Costs (eq 7).⁴⁵

item	ref year	ref cost, P_A (GBP)	capacity basis	ref capacity, S_A	n	f (%)
R-101	2007	29259	volume (m ³)	3.00	0.53	10.33
R-102	2007	29259	volume (m ³)	3.00	0.53	10.33
R-103	2007	273079	volume (m ³)	3.00	0.68	10.33
pump	2015	958	–	–	–	–
cooler	2015	3454	–	–	–	–
mixer	2007	22230	power (kW)	5	0.30	10.33
crystallizer	2007	328875	volume (m ³)	10	0.22	10.33

process design results and insight into the comparative evaluation of batch versus continuous crystallization for nevirapine.

2.4. Process Material Efficiencies. Quantities of waste produced by different designs are compared via the popular green chemistry metric, the environmental factor (E-factor, E), defined as the ratio of the mass of waste to the mass of the desired product (i.e., the recovered API)^{42,43} (eq 6):

$$E = \frac{m_{\text{waste}}}{m_{\text{API}}} = \frac{m_{\text{uAPI}} + m_{\text{uS}} + m_{\text{ur}}}{m_{\text{API}}} \quad (6)$$

where m_{waste} is the total mass of waste, m_{API} and m_{uAPI} are the mass of recovered and unrecovered API, respectively, m_{uS} is the mass of unrecovered solvent, and m_{ur} is the mass of unreacted reagents.

2.5. Costing Methodology. We implement an established methodology for costing pharmaceutical manufacturing processes.⁵ All plant designs are assumed to be constructed and operated at an existing pharmaceutical manufacturing site with essential auxiliary structures already in place.

2.5.1. Capital Expenditure (CapEx). Prices of equipment with capacities similar to those considered here are sourced where possible; where such data are unavailable, the following cost–capacity correlation is used:⁴⁴

$$P_B = fP_A \left(\frac{S_B}{S_A} \right)^n \quad (7)$$

where P_j is the equipment purchase cost at capacity S_j and the parameters f and n are equipment-dependent and found in the literature.⁴⁵ Where the reference purchase cost (P_A) is taken from the past, chemical engineering plant cost indices (CEPCIs) are used to calculate the corresponding purchase cost in the year 2018. All equipment capacities are scaled to account for plantwide inefficiencies and to meet the specified plant capacity. Unit costs and values of the parameters f and n in eq 7 are given in previous work.^{5,46} Unit operations similar to those implemented in the demonstrated continuous flow synthesis¹⁰ were implemented, scaled, and costed using published eq 7 parameters.⁴⁵ Table 4 gives details of the purchase costs and scaling parameters in eq 7 for each equipment item.

The sum of all inflation-adjusted equipment costs (P_B) gives the free-on-board cost (FOB). The Chilton method is used to calculate the battery limits installed cost (BLIC).⁴⁴ The installed equipment cost (IEC), process piping and instrumentation cost (PPI), and total physical plant cost (TPPC) are calculated from eqs 8–10. A construction factor of 30% is added to the TPPC to calculate the BLIC (eq 11).

$$\text{IEC} = 1.43 \cdot \text{FOB} \quad (8)$$

$$\text{PPI} = 0.42 \cdot \text{IEC} \quad (9)$$

$$\text{TPPC} = \text{IEC} + \text{PPI} \quad (10)$$

$$\text{BLIC} = 1.3 \cdot \text{TPPC} \quad (11)$$

Working capital costs (WC) are taken as 35% and 3.5% of annual material costs scaled to meet the desired plant capacity ($\text{MAT}_{\text{annual}}$) for the batch and continuous processes, respectively (eq 12):

$$\text{WC} = \begin{cases} 0.350 \cdot \text{MAT}_{\text{annual}} & \text{for BX} \\ 0.035 \cdot \text{MAT}_{\text{annual}} & \text{for CPM} \end{cases} \quad (12)$$

Contingency costs (CC) are calculated as 20% of the BLIC (eq 13):

$$\text{CC} = 0.2 \cdot \text{BLIC} \quad (13)$$

The sum of the BLIC, WC, and CC gives the total capital expenditure (CapEx) (eq 14):

$$\text{CapEx} = \text{BLIC} + \text{WC} + \text{CC} \quad (14)$$

2.5.2. Operating Expenditure (OpEx). Required material prices are summarized in Table 5. Base-case prices for the

Table 5. Material Prices for Reagents and Components Used in Continuous API Synthesis and Crystallization

process	material	price (GBP kg ⁻¹)
synthesis	CAPIC	5.00
	diglyme	3.00
	MeCAN	10.00
crystallization	NaH	5.00
	AC	1.50
	HCl(aq)	0.50
	NaOH(aq)	0.25

starting materials CAPIC and MeCAN are assumed in this work. Current lab-scale demonstrations of batch syntheses of these starting materials estimate the prices of CAPIC and MeCAN to be higher;¹⁰ however, these estimations are made from batch synthesis material requirements using reagent-grade materials. On the basis of the larger scales of operation considered in this work, it can be assumed that the material prices will be lower. The annual utilities cost ($\text{UTIL}_{\text{annual}}$) is calculated as 0.96 GBP per kilogram of process material throughput (m_{process}) plus the cost of utilities for heating of R-103, obtained as the heating duty for R-103 (Q_{R103} , taken as the sensible heat required to heat the process stream from $T_{\text{R102}} = 65$ °C to T_{R103} assuming a heat loss of 20%) multiplied by an electricity cost of 0.1386 GBP kWh⁻¹:

$$\text{UTIL}_{\text{annual}} = 0.96m_{\text{process}} + 0.1386Q_{\text{R103}} \quad (15)$$

The assumed heat loss of 20% is a rather high estimate for the process scales considered here, and thus, overestimates of

utilities cost values may be present. The annual waste cost ($\text{Waste}_{\text{annual}}$) is 0.35 GBP per liter of waste (Q_{waste}):

$$\text{Waste}_{\text{annual}} = 0.35Q_{\text{waste}} \quad (16)$$

The annual operating expenditure ($\text{OpEx}_{\text{annual}}$) is the sum of the annual material, utilities, and waste costs:

$$\text{OpEx}_{\text{annual}} = \text{MAT}_{\text{annual}} + \text{UTIL}_{\text{annual}} + \text{Waste}_{\text{annual}} \quad (17)$$

2.5.3. Total Cost. The total cost of the plant design is calculated by addition of CapEx and the sum of inflation-adjusted $\text{OpEx}_{\text{annual}}$ over the plant lifetime (eq 18):

$$\text{Total Cost} = \text{CapEx} + \sum_{j=1}^{20} \frac{\text{OpEx}_{\text{annual}}}{(1+y)^j} \quad (18)$$

in which a plant operating lifetime of 20 yr and an interest rate (y) of 5% are considered. All of the CapEx is assumed to occur in year 0, and operation is assumed to begin in year 1. Annual operation of 8000 h per year is assumed for consistency with our previously published work in this field. The assumed annual operation time can easily be altered by an expert reader to account for varying asset utilization efficiencies in the presented modeling framework.

2.6. Nonlinear Optimization Formulation. The objective of the optimization problem is to minimize the plantwide total cost subject to constraints on the continuous decision variables (eqs 19–21):

$$\min \text{Total Cost} \quad (19)$$

such that

$$120 \text{ }^\circ\text{C} \leq T_{\text{R103}} \leq 165 \text{ }^\circ\text{C} \quad (20)$$

$$1 \leq \text{pH}_{\text{CRYST}} \leq 7 \quad (21)$$

The decision variables are the operating temperature of R-103, T_{R103} , and the crystallization pH, pH_{CRYST} , which influence the final API yield by influencing the conversion of CYCLOR to the API in R-103 and the crystallization yield, respectively. While increasing T_{R103} enhances the conversion of CYCLOR to the API, there are utilities costs associated with heating R-103 (eq 15) that contribute to OpEx and the plant total cost. Similarly, increasing pH_{CRYST} increases the crystallization yield but also incurs higher material costs as well as larger crystallization capacities, which contribute to the total cost.

The constraints on the R-103 operating temperature are chosen to be the lower and upper bounds of available temperature data for Arrhenius parameter estimation (120 and 165 °C, respectively; eq 20) in order to ensure validity of the regressed parameters for subsequent modeling and optimization. The constraints on the crystallization pH (eq 21) were chosen to be $\text{pH}_{\text{CRYST}} = 1$ (close to the feed mixture pH of ~0.5) and $\text{pH}_{\text{CRYST}} = 7$ (the BX crystallization pH).

The optimization problem was solved in MATLAB using the interior-point algorithm with tolerances of 10^{-6} . Plant capacities (Q_{API}) of 10^2 and 10^3 kg of API yr^{-1} were investigated to represent small-scale and pilot-scale designs, respectively, and to be consistent with our previous publications.^{5,46–48} The effect of solvent recovery (SR) was also considered, as this has a significant effect on material consumption and thus material cost contributions toward OpEx. Solvent recovery of 80% is reported in the literature;¹⁰ however, the attainable SR may be lower in practice, so lower values of 0 and 40% were also considered in this work.

The nonlinear optimization problem was solved for all individual combinations of plant capacity ($Q_{\text{API}} = \{10^2, 10^3\}$ kg of API yr^{-1}) and assumed solvent recovery ($\text{SR} = \{0, 40, 80\}\%$), i.e., six problem instances, in order to avoid mixed-integer problem formulations and reduce the complexity of the optimization problem. Multiple initial values for decision variables were tested to ensure a unique optimal solution for each problem instance. The initial values of the decision variables for each problem instance were $T_{\text{R103},0} = \{130, 145, 160\}$ °C and $\text{pH}_{\text{CRYST},0} = \{2, 4, 6\}$, i.e., a total of nine initial points per problem instance. Unique solutions were attained for all of the problem instances independent of the different decision variable initial values. The solution times were short for all of the problem instances (Table 6).

Table 6. Optimization Problem Solution Times for Different Problem Instances

Q_{API} (kg of API yr^{-1})	SR (%)	solution time (s)
10^2	0	14.5
	40	19.5
	80	7.8
10^3	0	8.7
	40	7.5
	80	7.4

3. RESULTS AND DISCUSSION

3.1. Total Cost Response Surfaces and Optimal Operating Conditions. Cost response surfaces under different design assumptions were generated (Figure 8) to investigate the design space and to ensure that multiple cost minima were not present. The cost response surfaces for all of the design cases show a sharp peak (i.e., very high total cost) at low R-103 operating temperature (T_{R103}) and low crystallization pH (pH_{CRYST}). Under these conditions, very low API recovery is attained, and thus, higher material requirements and unit operation capacities are required to meet the desired plant capacity (Q_{API}), resulting in high CapEx and OpEx. At higher Q_{API} , the response surfaces take a similar shape but present higher total cost values due to the increased material throughput and correspondingly larger unit operation scales. Varying solvent recovery is also shown to significantly affect the cost response surfaces because of its effect on material requirements (as the solvent is a major contributor to the mixture composition) and thus on OpEx components as well as waste.

The optimal values of the decision variables (T_{R103} and pH_{CRYST}) corresponding to minimum total costs under different design assumptions are shown in Figure 9. These optima are compared to the process implementing a batch (BX) crystallization, where $T_{\text{R103}} = 165$ °C and $\text{pH}_{\text{CRYST}} = 7$. In all of the BX and continuous crystallization (CPM) design cases, T_{R103} is at the upper bound of 165 °C. The optimum crystallization pH varies across different CPM design assumptions. At lower solvent recovery ($\text{SR} = 0\%$), an optimum pH of ~4 is observed for both considered capacities; at low SR, OpEx components are significant contributors to the total cost, and thus, higher crystallization yields are preferred to lower the total cost. For higher SR (40 and 80%), pH_{CRYST} is driven to the lower bound of 1; the effect of enhancing the crystallization yield by increasing pH_{CRYST} is not as important when a significant percentage of the solvent is

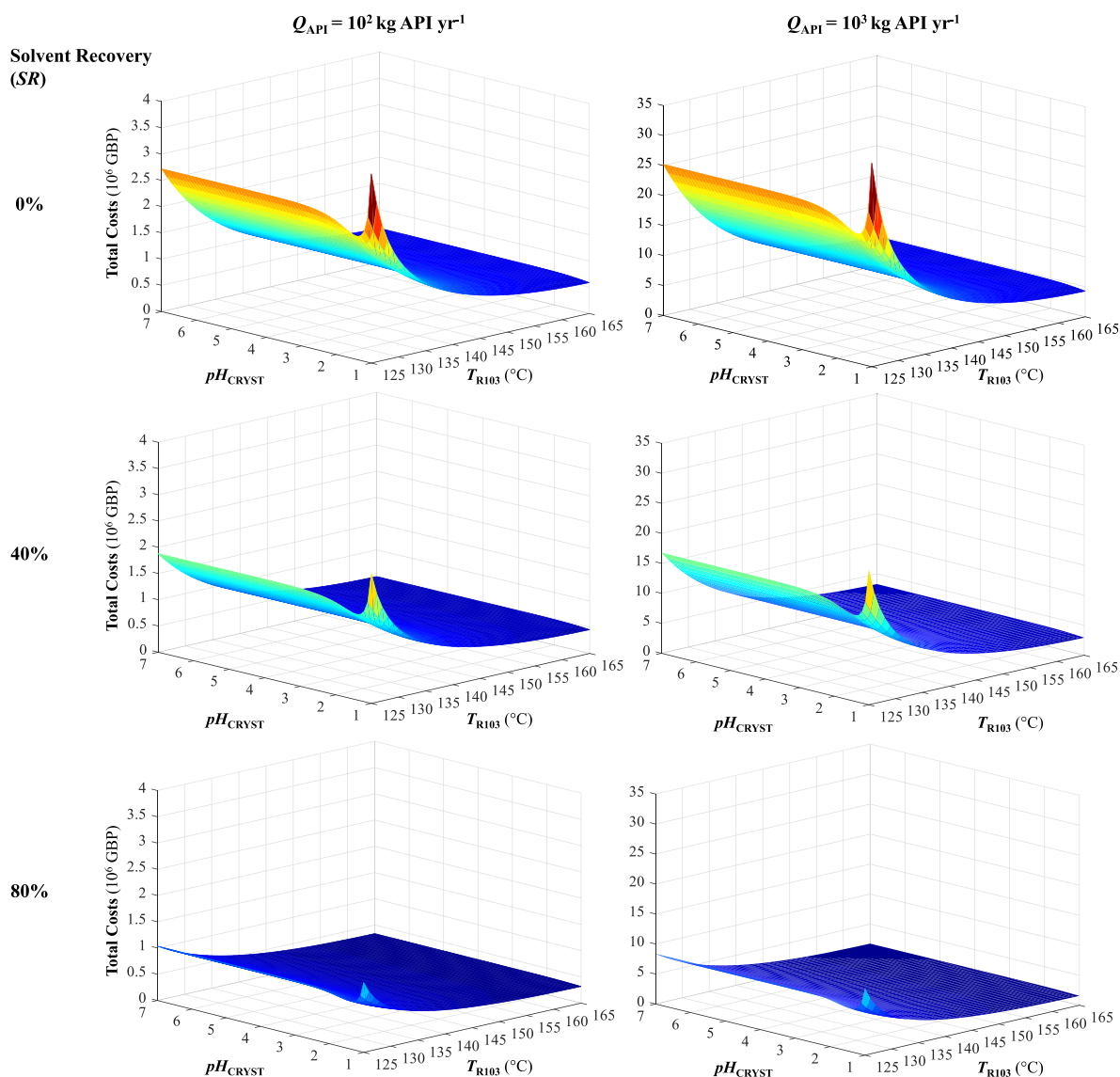


Figure 8. Total cost response surfaces for nevirapine CPM under different design assumptions of plant capacity (Q_{API}) and solvent recovery (SR).

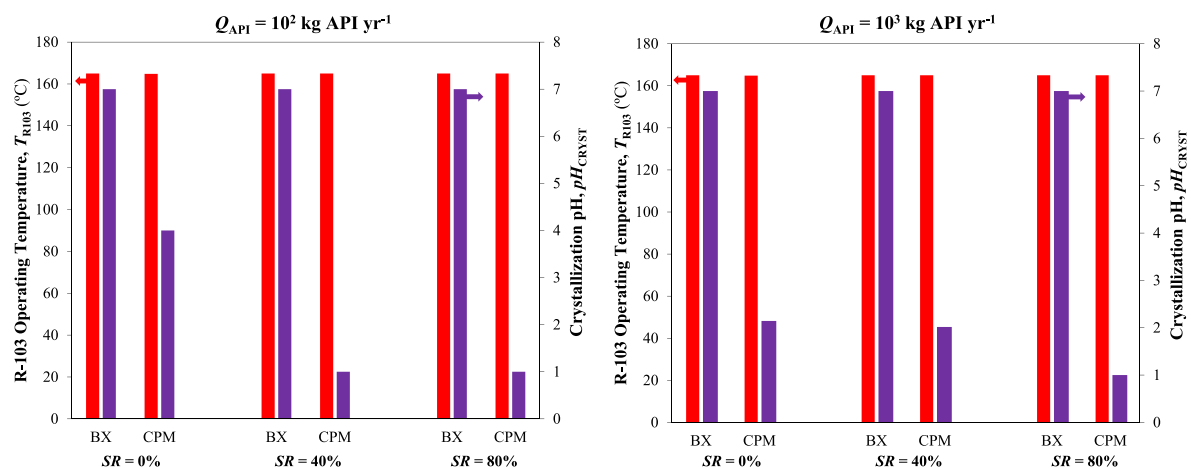


Figure 9. Optimal operating (decision) variables corresponding to the total cost minima under different design assumptions.

recovered and T_{R103} is high. At higher capacity ($Q_{API} = 10^3$ kg of API yr^{-1}), higher solvent recovery is required to allow a lower pH at the cost optimum. In industrial practice, for safety

purposes it may be necessary to neutralize the mixture following crystallization and API crystal removal, but this was not considered as part of the presented analysis.

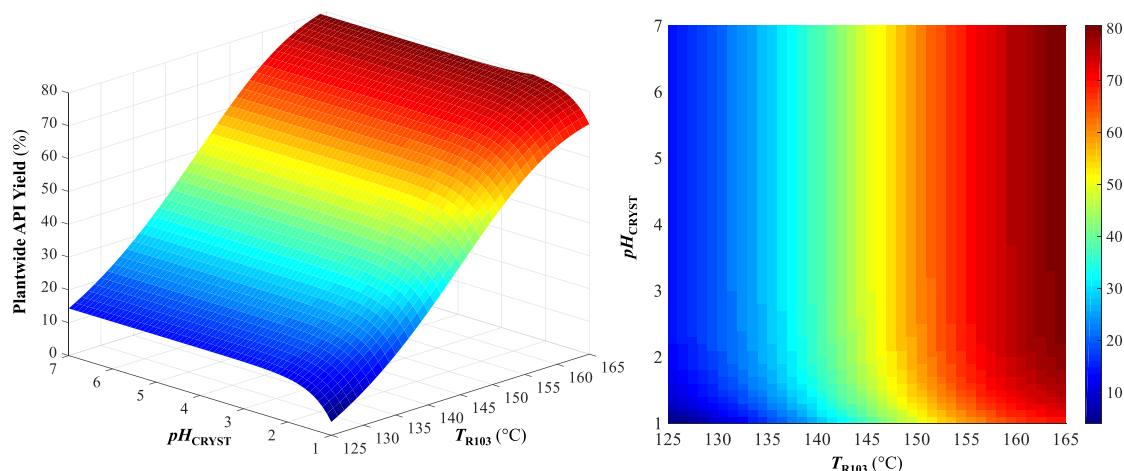


Figure 10. Response surface of plantwide API yield vs R-103 operating temperature (T_{R103}) and crystallization pH (pH_{CRYST}).

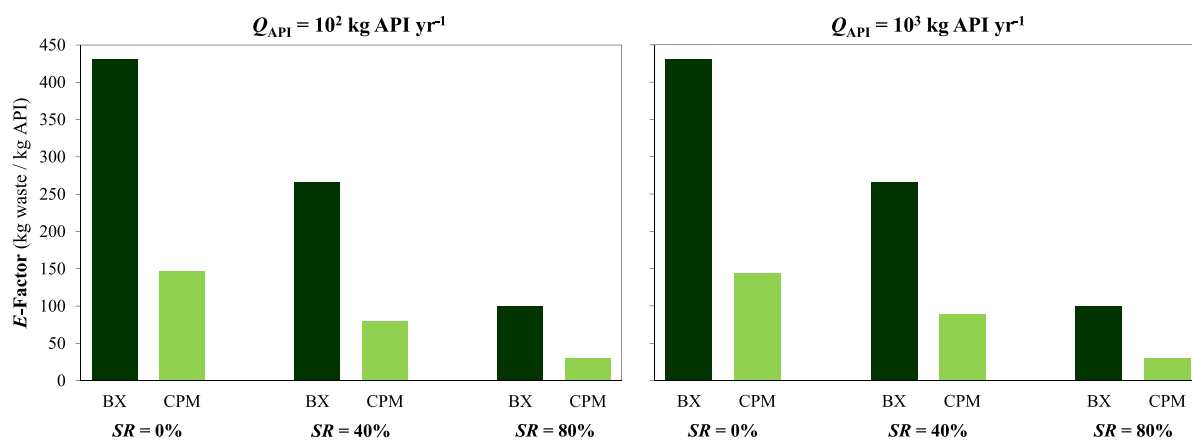


Figure 11. E-factors at cost optima for different design assumptions.

The effect of T_{R103} on the total cost is significant: the total cost decreases rapidly as T_{R103} increases from 125 to 165 °C (Figure 8). The operating temperature in R-103 significantly affects the conversion of CYCLOR to API, and thus, the plantwide API yield is very sensitive to T_{R103} ; expensive reagents, especially the starting materials CAPIC and MeCAN, make materials costs a major contributor to the total cost, and therefore, a high API yield in R-103 (i.e., high T_{R103}) is preferred. The effect of each decision variable (T_{R103} and pH_{CRYST}) on the plantwide API yield is shown in Figure 10 to illustrate this point. The optimization problem formulation in this work could alternatively be defined to maximize net present value (NPV), which may yield different results. However, problem formulation for NPV maximization requires the estimation of product sales revenues, which will vary with design assumption (see section 3.4 for estimated API costs of goods for different plant designs). For this reason, the objective is instead to minimize plant total costs. Comparison of results for a different objective function formulation could be useful given the availability of reliable projected API and brand sales prices.

The effect of pH_{CRYST} on the total cost is also similar across different design assumptions (Figure 8). At the lower bound of the R-103 operating temperature ($T_{R103} = 125$ °C), low pH (e.g., at the lower bound, $pH_{CRYST} = 1$) results in high total costs. At low T_{R103} , the low conversion of CYCLOR to API in R-103 means the plantwide yield is already poor prior to

crystallization; low pH_{CRYST} implies a lower crystallization yield, and thus, higher total costs are incurred because of increased material requirements and unit operation scales needed to meet the desired plant capacity. The implemented model of aqueous API solubility versus pH (eq 4 and Figure 7) shows a plateau in solubility beyond some pH value below 7. Increasing the crystallization pH too high will result in incremental increases in API yield at best (as shown in Figure 10), which will unnecessarily increase material usage and crystallization volumes and thus the total cost (as observed in the cost response surfaces in Figure 8). At the upper bound of R-103 operating temperature ($T_{R103} = 165$ °C), the effect of the crystallization pH is not so significant. The yield of the API is already high when T_{R103} is higher (because of increased conversion of CYCLOR to API in R-103), and thus, the effect of higher pH in the crystallization is not so important. This point is also further illustrated by the plantwide API yield response surface in Figure 10.

The current work optimized only the CPM process and did not optimize the batch process. Optimization of the batch process with respect to the decision variables considered here (T_{R103} and pH_{CRYST}) as well as batch scheduling and numbering would allow a fairer comparison with the CPM designs and should be implemented in future work.⁴⁹ Furthermore, implementation of process analytical technology (PAT) is essential for the success of CPM technologies, as it ensures that the operating variables do not deviate from their

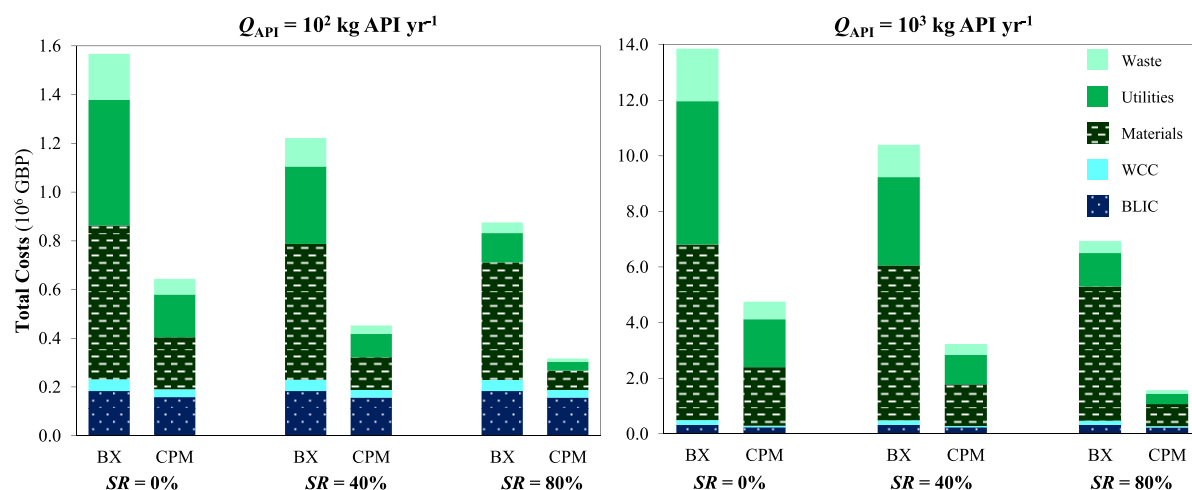


Figure 12. Total cost components for different design assumptions.

Table A1. Total Cost Components (10^6 GBP) and CPM Savings with Respect to BX (%)

	SR = 0%			SR = 40%			SR = 80%		
	BX	CPM	savings	BX	CPM	savings	BX	CPM	savings
$Q_{API} = 10^2$ kg of API yr ⁻¹									
BLIC	0.183	0.159	-13.52	0.183	0.157	-14.64	0.183	0.157	-14.64
WCC	0.048	0.032	-32.76	0.046	0.032	-32.06	0.045	0.031	-30.32
CapEx	0.231	0.191	-17.49	0.230	0.188	-18.16	0.229	0.188	-17.74
materials	0.632	0.214	-66.18	0.557	0.134	-75.98	0.483	0.079	-83.60
utilities	0.516	0.175	-66.03	0.318	0.096	-69.94	0.120	0.037	-69.61
waste	0.189	0.064	-66.03	0.116	0.035	-69.94	0.044	0.013	-69.61
OpEx	1.336	0.453	-66.10	0.992	0.264	-73.33	0.647	0.129	-80.05
total costs	1.567	0.644	-58.93	1.221	0.453	-62.95	0.876	0.317	-63.78
$Q_{API} = 10^3$ kg of API yr ⁻¹									
BLIC	0.320	0.235	-26.51	0.320	0.235	-26.58	0.320	0.229	-28.46
WCC	0.174	0.051	-70.95	0.161	0.050	-69.31	0.148	0.047	-68.25
CapEx	0.494	0.286	-42.20	0.481	0.284	-40.92	0.468	0.276	-41.08
materials	6.316	2.109	-66.62	5.573	1.491	-73.24	4.830	0.792	-83.60
utilities	5.160	1.730	-66.47	3.181	1.065	-66.51	1.202	0.365	-69.61
waste	1.886	0.632	-66.47	1.162	0.389	-66.50	0.438	0.133	-69.61
OpEx	13.362	4.471	-66.54	9.916	2.946	-70.29	6.470	1.291	-80.05
total costs	13.856	4.757	-65.67	10.397	3.230	-68.93	6.939	1.567	-77.42

optimal values, thereby ensuring minimum total costs. Recent studies have illustrated the importance of PAT in crystallization applications.⁵⁰

3.3. Material Efficiencies. Material efficiencies of different design assumptions, as quantified by the E-factor (eq 6), are shown in Figure 11. For all of the batch designs, the E-factor values are very high, even for pharmaceutical processing, which is renowned for having highly material-intensive manufacturing routes;⁵¹ this is due to the fact that all of the batch crystallization processes operate at $pH_{CRYST} = 7$, requiring significant quantities of base to neutralize the feed mixture. In all cases, increasing the solvent recovery significantly reduces the E-factor because of the large contribution of the solvent to the process mixture and waste compositions. For pharmaceutical manufacturing, the E-factor can be as high as 200; all of the CPM designs achieve values lower than this, but only higher solvent recoveries allow this for the process with a batch crystallization. Determination of attainable solvent recoveries at different production scales will further clarify the likely material efficiencies of different design assumptions to elucidate materially efficient CPM plant designs.

3.4. Total Cost Components and API Cost of Goods.

The minimum total cost components for CPM are compared with those for the process with the BX crystallization in Figure 12 (also see Table A1, Appendix A). The total costs at $Q_{API} = 10^3$ kg of API yr⁻¹ are higher, reflecting the increased material requirements and unit operation scales. OpEx components are more significant than CapEx in all design cases because of the expensive reagents required for the API synthesis. As solvent recovery increases, the OpEx components decrease significantly, substantially lowering the total costs. Utilities and waste components are the most significantly affected by varying solvent recovery because of the large quantity of solvent in the process mixture; materials costs are less affected by varying solvent recovery, as the reagents used are much more expensive than the solvent components in the considered process (see Table 5). In all cases, CPM designs have significantly lower OpEx components than BX designs because of the reduced material requirements of the crystallization process operating at lower pH. The costing methodology implemented here does not include labor requirements, which

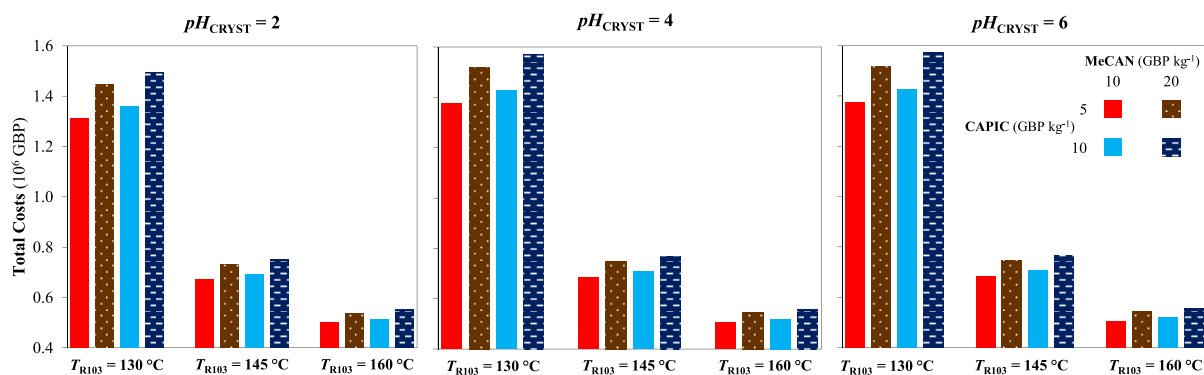


Figure 13. Effect of starting material prices and T_{R103} and pH_{CRYST} on plant total costs ($Q_{API} = 10^2$ kg of API yr⁻¹, SR = 40%).

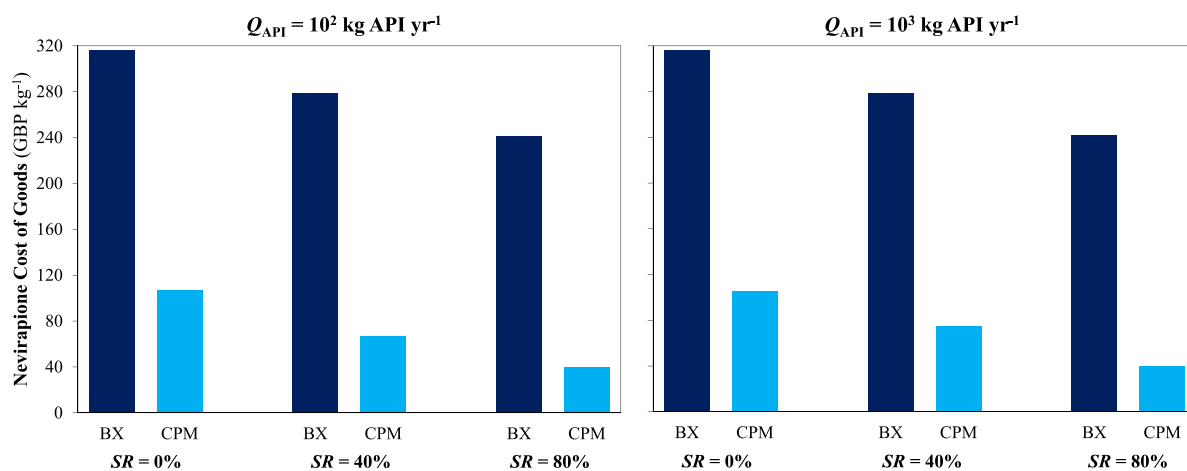


Figure 14. Estimated API costs of goods from total costs of different plant designs.

are location- and scale-dependent; elucidation of labor costs will further inform process development.

For varying solvent recovery assumptions, the CapEx components remain roughly the same, as the internal process stream flow rates through each unit operation remain fairly consistent. In all cases, CPM designs have lower CapEx components than their BX counterparts because of the lower material throughputs of these processes. The availability of detailed crystallization kinetic models with experimental data and model parameters can further elucidate crystallization process performance and unit operation design, which will likely have a significant effect on CapEx. The equipment cost correlation used here (eq 7) is the most widely implemented and reliable one available in the peer-reviewed literature; the design capacities required for the considered plant capacities (Q_{API}) are at the lower end of the cost correlation application range, and thus, purchase cost overestimation may be present. Additional uncertainty in the calculated unit purchase costs is present because of the lack of cost estimation methods for specific equipment. The correlation is the one most widely implemented in the literature to scale equipment purchase costs versus capacity for different types of unit operations. For some specialized unit operations, specific cost correlations have been established,⁵² which may be more accurate than the general correlation used in this work. Cost correlations specific to particular unit operations should be used where possible to allow accurate prediction of CapEx component contributions to total costs. Furthermore, the considered processes (both BX and CPM) are considered to take advantage of being

constructed at an existing pharmaceutical manufacturing site; additional costs may also be incurred if green-field construction is required.

The starting materials (CAPIC and MeCAN) for the continuous synthesis of nevirapine considered in this work are advanced compounds synthesized by multistep batch processes.¹⁰ Consideration of key material price fluctuations is an important form of sensitivity analysis that should be implemented in modeling and economic evaluation during candidate process screening and development stages.⁵ Here we consider the effect of increasing the CAPIC and MeCAN material prices by 50% from the base-case values (Table 2) on plant total costs, i.e., CAPIC price = [5, 10] GBP kg⁻¹, MeCAN price = [10, 20] GBP kg⁻¹, at discrete values of the decision variables, i.e., $T_{R103} = \{130, 145, 160\}$ °C and $pH_{CRYST} = \{2, 4, 6\}$ for $Q_{API} = 10^2$ kg of API yr⁻¹ and SR = 40%; the observed trends are expected to be the same for alternative values of Q_{API} and SR. The effects of varying material prices for these discrete decision variable values are shown in Figure 13. Although the starting material prices do affect the total plant cost in all design cases, the effect of T_{R103} is still the most sensitive parameter affecting the total cost. Further process intensification for the batchwise syntheses of CAPIC and MeCAN will ensure reasonable material prices, thereby ensuring the economic viability of the process designs investigated here.

3.5. API Cost of Goods. In all cases, CPM designs are more economically viable than those implementing a BX crystallization. The cost component savings for each process

with respect to the corresponding BX design are shown in Table A1 in Appendix A. The most significant savings are realized in OpEx components (materials, utilities, and waste components, as described in the costing methodology), which allow significant total savings because of their large contribution to plant total costs. Ensuring affordable, accessible HIV medicines is essential; HIV drug unit prices have varied widely in previous years, so quantifying the attainable price per unit mass is an important consideration for HIV drug manufacturing.⁵³ The cost of goods (CoG) of the API is calculated to quantitatively compare differences in affordability of nevirapine under different design assumptions. The CoG is calculated as the total mass of API produced during the plant operating lifetime (t) divided by the total cost of constructing and operating the plant:

$$\text{CoG} = \frac{Q_{\text{API}} t}{\text{Total Cost}} \quad (22)$$

The resulting API CoG values under different design assumptions are presented in Figure 14. For all cases, CPM designs allow lower API CoG than their batch alternatives because of the significant total cost savings allowed by continuous operation. Solvent recovery has a significant effect on the resulting CoG because of the large contribution of solvent to OpEx components, which dominate the total costs of all design cases. While this analysis does not clarify exactly the price at which the API will be sold, the estimated CoG values indicate that CPM implementation can allow for lower API sale prices to expand global access to this societally important HIV drug.

4. CONCLUSIONS

This paper presents the formulation and solution of a nonlinear optimization problem⁵⁴ for minimization of the total cost of plantwide CPM of nevirapine, a societally important API for HIV-1 treatment. Optimization of a conceptual continuous crystallization for the purification of the API synthesis effluent following the continuous flow synthesis under various design assumptions (plant capacity and solvent recovery) is used to quantitatively evaluate different designs for nevirapine CPM. The operating temperature of the final reactor R-103 is driven to the upper bound in all design cases to maximize the API synthesis yield, while the crystallization pH for CPM designs is always lower than that of the batch crystallization (pH 7) to minimize major OpEx contributions to plant total costs. In all of the design cases, CPM designs achieve lower total cost components, improved material efficiencies, and lower API CoG values, demonstrating the promise of CPM over batch for nevirapine production and improving global, affordable access to HIV APIs. This work also demonstrates the value of conducting technoeconomic optimization studies toward the development of continuous processes in pursuit of economically viable end-to-end CPM plants.

■ APPENDIX A. TOTAL COST COMPONENTS AND COST SAVINGS

Table A1 details total cost optima component values for both BX and CPM designs and CPM savings with respect to BX crystallization implementation.

■ AUTHOR INFORMATION

Corresponding Author

*E-mail: D.Gerogiorgis@ed.ac.uk. Phone: + 44 131 6517072.

ORCID

Dimitrios I. Gerogiorgis: [0000-0002-2210-6784](https://orcid.org/0000-0002-2210-6784)

Notes

Tabulated and cited literature data suffice for reproduction of all original process simulation and optimization results, and no other supporting data are required to ensure reproducibility. The authors declare no competing financial interest.

■ ACKNOWLEDGMENTS

S.D. gratefully acknowledges the financial support of the Engineering and Physical Sciences Research Council (EPSRC) via a Doctoral Training Partnership (DTP) Ph.D. Fellowship (Grant EP/N509644/1) and the Royal Society of Edinburgh for a John Moyes Lessells Travel Scholarship to visit Virginia Commonwealth University. D.I.G. gratefully acknowledges a Royal Academy of Engineering (RAEng) Industrial Fellowship.

■ NOMENCLATURE AND ACRONYMS

Acronyms

API	active pharmaceutical ingredient
BX	batch
CEPCI	chemical engineering plant cost index
CPM	continuous pharmaceutical manufacturing
HIV	human immunodeficiency virus
LLE	liquid–liquid extraction
NPV	net present value
PAT	process analytical technology
PBR	packed bed reactor
WHO	World Health Organization

Variables

Latin Letters

A	pre-exponential factor
BLIC	battery limits installed cost (GBP)
C_{CRYST}	concentration of API in the crystallization mother liquor (g L^{-1})
$C_{i,0}$	initial concentration of reagent i (M)
CapEx	capital expenditure (GBP)
CC	contingency costs (GBP)
CoG	cost of goods (GBP kg^{-1})
E	E-factor
E_a	activation energy (J mol^{-1})
f	correction factor in eq 7
$F_{A,0}^j$	molar flow rate of limiting reagent A entering reactor j (mol s^{-1})
F_i^j	molar flow rate of component i exiting reactor j (mol s^{-1})
FOB	free-on-board cost (GBP)
IEC	installed equipment cost (GBP)
k	first-order reaction rate constant of R-103 (s^{-1})
m_{API}	mass of recovered API (kg yr^{-1})
m_{process}	plant material throughput (kg yr^{-1})
m_{ur}	mass of reagents remaining in waste streams (kg yr^{-1})
m_{uAPI}	mass of unrecovered API (kg yr^{-1})
m_{uS}	mass of unrecovered solvent (kg yr^{-1})
m_{waste}	mass of waste (kg yr^{-1})
$\text{MAT}_{\text{annual}}$	annual material costs (GBP yr^{-1})
n	exponent in eq 7

OpEx _{annual}	annual operating expenditure (GBP yr ⁻¹)
P _j	equipment purchase cost at capacity <i>j</i> (GBP)
pH _{CRYST}	crystallization pH
pH _{CRYST,0}	initial value of the crystallization pH in problem formulation
PPI	process piping and instrumentation cost (GBP)
Q _{API}	plant API capacity (kg of API yr ⁻¹)
Q _{R103}	heating duty of R-103 considering 20% heat loss (kWh)
Q _{waste}	volumetric flow of waste output (L yr ⁻¹)
R	universal gas constant (8.314 J mol ⁻¹ K ⁻¹)
R ²	coefficient of determination
S	aqueous API solubility (g of API L ⁻¹)
S _j	capacity of equipment <i>j</i> (varying units)
S ₀	nonionized aqueous API solubility (g of API L ⁻¹)
SR	solvent recovery (%)
T _i	operating temperature of reactor <i>i</i> (°C)
T _{R103,0}	initial value of R-103 operating temperature in problem formulation (°C)
<i>t</i>	plant operation lifetime (yr)
TPPC	total physical plant cost (GBP)
UTIL _{annual}	annual utilities cost (GBP yr ⁻¹)
V _j	volume of unit <i>j</i> (m ³)
Waste _{annual}	annual waste disposal cost (GBP yr ⁻¹)
WC	working capital costs (GBP)
X _A	conversion of limiting reagent A in reactor <i>j</i> (%)
Y	crystallization yield (%)
<i>y</i>	interest rate (%)

Greek Letters

Θ _i ^j	molar ratio of excess reagent <i>i</i> to limiting reagent in reactor <i>j</i>
ν _i	stoichiometric coefficient of reagent <i>i</i> in reactor <i>j</i>
τ	residence time (s)

Molecules and Reagents

2-CAN	2-(cyclopropylamino)nicotinic acid
AC	activated carbon
Ac ₂ O	acetic anhydride
Al ₂ O ₃	aluminum oxide
CAPIC	2-chloro-3-amino-4-picoline
CAPIC-Na	CAPIC sodium salt
COMAD	2-chloro-4-methylnicotinamide
CPA	cyclopropylamine
CYCIC	2-chloro-4-methylnicotinonitrile
CYCLOR	<i>N</i> -(2-chloro-4-methylpyridin-3-yl)-2-(cyclopropylamino)nicotinamide
DMF–DMS	dimethylformamide–dimethyl sulfate
H ₂ SO ₄	sulfuric acid
HCl	hydrogen chloride
IPA	isopropyl alcohol
KOH	potassium hydroxide
MeCAN	methyl 2-(cyclopropylamino)nicotinate
MeOH	methanol
Mg ₂ SO ₄	magnesium sulfate
NaH	sodium hydride
NaOBr	sodium hypobromite
NaOH	sodium hydroxide
PhMe	toluene
SOCl ₂	thionyl chloride
TEA	triethylamine

REFERENCES

- (1) Fortunak, J. M.; de Souza, R. O. M. A.; Kulkarni, A. A.; King, C. L.; Ellison, T.; Miranda, L. S. M. Active pharmaceutical ingredients for antiretroviral treatment in low- and middle-income countries: a survey. *Antiviral Ther.* **2014**, *19* (3), 15–29.
- (2) UNAIDS Data 2018; UNAIDS: Geneva, 2018.
- (3) Schwab, K. *The Global Competitiveness Report 2017/2018*; World Economic Forum: Geneva, 2017.
- (4) Dallinger, D.; Kappe, C. O. Why flow means green – Evaluating the merits of continuous processing in the context of sustainability. *Curr. Opin. Green Sustainable Chem.* **2017**, *7*, 6–12.
- (5) Jolliffe, H. G.; Gerogiorgis, D. I. Plantwide design and economic evaluation of two continuous pharmaceutical manufacturing (CPM) cases: ibuprofen and artemisinin. *Comput. Chem. Eng.* **2016**, *91*, 269–288.
- (6) de Souza, R. O. M. A.; Watts, P. Flow processing as a tool for API production in developing economies. *J. Flow Chem.* **2017**, *7* (3), 146–150.
- (7) Gérardy, R.; Emmanuel, N.; Toupy, T.; Kassim, V. E.; Tshibalonza, N. N.; Schmitz, M.; Monbaliu, J. C. M. Continuous flow organic chemistry: successes and pitfalls at the interface with current societal challenges. *Eur. J. Org. Chem.* **2018**, *2018* (20–21), 2301–2351.
- (8) Britton, J.; Raston, C. L. Multi-step continuous-flow synthesis. *Chem. Soc. Rev.* **2017**, *46* (5), 1250–1271.
- (9) Baxendale, I. R.; Braatz, R. D.; Hodnett, B. K.; Jensen, K. F.; Johnson, M. D.; Sharratt, P.; Sherlock, J. P.; Florence, A. J. Achieving continuous manufacturing: technologies and approaches for synthesis, workup, and isolation of drug substance. *J. Pharm. Sci.* **2015**, *104* (3), 781–791.
- (10) Verghese, J.; Kong, C. J.; Rivalti, D.; Yu, E. C.; Krack, R.; Alcázar, J.; Manley, J. B.; McQuade, D. T.; Ahmad, S.; Belecki, K.; Gupton, B. F. Increasing global access to the high-volume HIV drug nevirapine through process intensification. *Green Chem.* **2017**, *19* (13), 2986–2991.
- (11) Longstreet, A. R.; Opalka, S. M.; Campbell, B. S.; Gupton, B. F.; McQuade, D. T. Investigating the continuous synthesis of a nicotinonitrile precursor to nevirapine. *Beilstein J. Org. Chem.* **2013**, *9*, 2570–2578.
- (12) Longstreet, A. R.; Campbell, B. S.; Gupton, B. F.; McQuade, D. T. Improved synthesis of mono- and disubstituted 2-halonicotinonitriles from alkylidene malononitriles. *Org. Lett.* **2013**, *15* (20), 5298–5301.
- (13) Teoh, S. K.; Rathi, C.; Sharratt, P. Practical assessment methodology for converting fine chemicals processes from batch to continuous. *Org. Process Res. Dev.* **2016**, *20* (2), 414–431.
- (14) Bana, P.; Örkényi, R.; Lövei, K.; Lakó, A.; Túrós, G. I.; Éles, J.; Faigl, F.; Greiner, I. The route from problem to solution in multistep continuous flow synthesis of pharmaceutical compounds. *Bioorg. Med. Chem.* **2017**, *25* (23), 6180–6189.
- (15) Jolliffe, H. G.; Diab, S.; Gerogiorgis, D. I. Nonlinear optimization via explicit NRTL model solubility prediction for antisolvent mixture selection in artemisinin crystallization. *Org. Process Res. Dev.* **2018**, *22* (1), 40–53.
- (16) Grom, M.; Stavber, G.; Drnovšek, P.; Likozar, B. Modelling chemical kinetics of a complex reaction network of active pharmaceutical ingredient (API) synthesis with process optimization for benzazepine heterocyclic compound. *Chem. Eng. J.* **2016**, *283*, 703–716.
- (17) Patel, M. P.; Shah, N.; Ashe, R. Robust optimization methodology for the process synthesis of continuous technologies. *Comput.-Aided Chem. Eng.* **2011**, *29*, 351–355.
- (18) Bédard, A.-C.; Adamo, A.; Aroh, K. C.; Russell, M. G.; Bedermann, A. A.; Torosian, J.; Yue, B.; Jensen, K. F.; Jamison, T. F. Reconfigurable system for automated optimization of diverse chemical reactions. *Science* **2018**, *361* (6408), 1220–1225.
- (19) Ott, D.; Kralisch, D.; Denčić, I.; Hessel, V.; Laribi, Y.; Perrichon, P. D.; Berguerand, C.; Kiwi-Minsker, L.; Loeb, P. Life cycle analysis within pharmaceutical process optimization and intensifica-

tion: case study of active pharmaceutical ingredient production. *ChemSusChem* **2014**, *7* (12), 3521–3533.

(20) Ott, D.; Borukhova, S.; Hessel, V. Life cycle assessment of multi-step rufinamide synthesis – from isolated reactions in batch to continuous microreactor networks. *Green Chem.* **2016**, *18* (4), 1096–1116.

(21) Drageset, A.; Bjørsvik, H.-R. Continuous flow synthesis concatenated with continuous flow liquid–liquid extraction for work-up and purification: selective mono- and di-iodination of the imidazole backbone. *React. Chem. Eng.* **2016**, *1* (4), 436–444.

(22) Monbaliu, J.-C.M.; Stelzer, T.; Revalor, E.; Weeranoppanant, N.; Jensen, K. F.; Myerson, A. S. Compact and integrated approach for advanced end-to-end production, purification, and aqueous formulation of lidocaine hydrochloride. *Org. Process Res. Dev.* **2016**, *20* (7), 1347–1353.

(23) Weeranoppanant, N.; Adamo, A.; Sapparaiuly, G.; Rose, E.; Fleury, C.; Schenkel, B.; Jensen, K. F. Design of multistage counter-current liquid–liquid extraction for small-scale applications. *Ind. Eng. Chem. Res.* **2017**, *56* (14), 4095–4103.

(24) Yang, Y.; Nagy, Z. K. Combined cooling and antisolvent crystallization in continuous mixed suspension, mixed product removal cascade crystallizers: steady-state and startup optimization. *Ind. Eng. Chem. Res.* **2015**, *54* (21), 5673–5682.

(25) Ridder, B. J.; Majumder, A.; Nagy, Z. K. Population balance model-based multiobjective optimization of a multisegment multi-addition (MSMA) continuous plug-flow antisolvent crystallizer. *Ind. Eng. Chem. Res.* **2014**, *53* (11), 4387–4397.

(26) Li, J.; Lai, T. C.; Trout, B. L.; Myerson, A. S. Continuous crystallization of cyclosporine: the effect of operating conditions on yield and purity. *Cryst. Growth Des.* **2017**, *17* (3), 1000–1007.

(27) Acevedo, D.; Tandy, Y.; Nagy, Z. K. Multiobjective optimization of an unseeded batch cooling crystallizer for shape and size manipulation. *Ind. Eng. Chem. Res.* **2015**, *54* (7), 2156–2166.

(28) Ridder, B. J.; Majumder, A.; Nagy, Z. K. Parametric, optimization-based study on the feasibility of a multisegment antisolvent crystallizer for in situ fines removal and matching of target size distribution. *Ind. Eng. Chem. Res.* **2016**, *55* (8), 2371–2380.

(29) Park, K.; Kim, D. Y.; Yang, D. R. Operating strategy for continuous multistage mixed suspension and mixed product removal (MSMPR) crystallization processes depending on crystallization kinetic parameters. *Ind. Eng. Chem. Res.* **2016**, *55* (6), 7142–7153.

(30) Zhang, H.; Quon, J.; Alvarez, A. J.; Evans, J.; Myerson, A. S.; Trout, B. Development of continuous anti-solvent/cooling crystallization process using cascaded mixed suspension, mixed product removal crystallizers. *Org. Process Res. Dev.* **2012**, *16* (5), 915–924.

(31) Lee, J. W.; Horváth, Z.; O'Brien, A. G.; Seeberger, P. H.; Seidel-Morgenstern, A. Design and optimization of coupling a continuously operated reactor with simulated moving bed chromatography. *Chem. Eng. J.* **2014**, *251*, 355–370.

(32) Denčić, I.; Ott, D.; Kralisch, D.; Noel, T.; Meuldijk, J.; de Croon, M.; Hessel, V.; Laribi, Y.; Perrichon, P. Eco-efficiency analysis for intensified production of an active pharmaceutical ingredient: a case study. *Org. Process Res. Dev.* **2014**, *18* (11), 1326–1338.

(33) Correia, C. A.; Gilmore, K.; McQuade, D. T.; Seeberger, P. H. A concise flow synthesis of efavirenz. *Angew. Chem., Int. Ed.* **2015**, *54* (16), 4945–4948.

(34) Kuehn, S. E. Janssen embraces continuous manufacturing for Prezista (Oct 8, 2015). <http://www.pharmamanufacturing.com/articles/2015/janssen-embraces-continuous-manufacturing-for-prezista/> (accessed Nov 17, 2018).

(35) FDA approves tablet production on Janssen continuous manufacturing line (April 12, 2016). <http://www.pharmtech.com/fda-approves-tablet-production-janssen-continuous-manufacturing-line> (accessed Nov 17, 2018).

(36) Mandala, D.; Chada, S.; Watts, P. Semi-continuous multi-step synthesis of lamivudine. *Org. Biomol. Chem.* **2017**, *15* (16), 3444–3454.

(37) Ziegler, R. E.; Desai, B. K.; Jee, J.-A.; Gupton, B. F.; Roper, T. D.; Jamison, T. F. 7-step flow synthesis of the HIV integrase inhibitor dolutegravir. *Angew. Chem., Int. Ed.* **2018**, *57* (24), 7181–7185.

(38) Kuminek, G.; Rodríguez-Hornedo, N.; Siedler, S.; Rocha, H. V. A.; Cuffini, S. L.; Cardoso, S. G. How cocrystals of weakly basic drugs and acidic cofomers might modulate solubility and stability. *Chem. Commun.* **2016**, *52* (34), 5832–5835.

(39) Hargrave, K. D.; Proudfoot, J. R.; Grozinger, K. G.; Cullen, E.; Kapadia, S. R.; Patel, U. R.; Fuchs, V. U.; Mauldin, S. C.; Vitous, J.; Behnke, M. L.; Klunder, J. M.; Pal, K.; Skiles, J. W.; McNeil, D. W.; Rose, J. M.; Chow, G. C.; Skoog, M. T.; Wu, J. C.; Schmidt, G.; Engel, W. W.; Eberlein, W. G.; Saboe, T. D.; Campbell, S. J.; Rosenthal, A. S.; Adams, J. Novel non-nucleoside inhibitors of HIV-1 reverse transcriptase. 1. Tricyclic pyridobenzo- and dipyridodiazepinones. *J. Med. Chem.* **1991**, *34* (7), 2231–2241.

(40) Macha, S.; Yong, C. L.; Darrington, T.; Davis, M. S.; MacGregor, T. R.; Castles, M.; Krill, S. L. In vitro-in vivo correlation of nevirapine extended release tablets. *Biopharm. Drug Dispos.* **2009**, *30* (9), 542–550.

(41) Cheeseman, S. H.; Hattox, S. E.; McLaughlin, M. M.; Koup, R. A.; Andrews, C.; Bova, C. A.; Pav, J. W.; Roy, T.; Sullivan, J. L.; Keirns, J. J. Pharmacokinetics of nevirapine: initial single-rising-dose study in humans. *Antimicrob. Agents Chemother.* **1993**, *37* (2), 178–82.

(42) Sheldon, R. A. Fundamentals of green chemistry: efficiency in reaction design. *Chem. Soc. Rev.* **2012**, *41* (4), 1437–1451.

(43) Roschangar, F.; Sheldon, R. A.; Senanayake, C. H. Overcoming barriers to green chemistry in the pharmaceutical industry – the Green Aspiration Level™ concept. *Green Chem.* **2015**, *17* (2), 752–768.

(44) Couper, J. R. *Process Engineering Economics*; CRC Press: Boca Raton, FL, 2003.

(45) Woods, D. R. *Rules of Thumb in Engineering Practice*; Wiley-VCH: Weinheim, Germany, 2007.

(46) Diab, S.; Gerogiorgis, D. I. Process modeling, simulation, and technoeconomic evaluation of separation solvents for the continuous pharmaceutical manufacturing (CPM) of diphenhydramine. *Org. Process Res. Dev.* **2017**, *21* (7), 924–946.

(47) Jolliffe, H. G.; Gerogiorgis, D. I. Technoeconomic optimization and comparative environmental impact evaluation of continuous crystallisation and antisolvent selection for artemisinin recovery. *Comput. Chem. Eng.* **2017**, *103*, 218–232.

(48) Diab, S.; Gerogiorgis, D. I. Process modelling, simulation and technoeconomic evaluation of crystallisation antisolvents for the continuous pharmaceutical manufacturing of rufinamide. *Comput. Chem. Eng.* **2018**, *111*, 102–114.

(49) Papavasileiou, V.; Koulouris, A.; Siletti, C.; Petrides, D. Optimize manufacturing of pharmaceutical products with process simulation and production scheduling tools. *Chem. Eng. Res. Des.* **2007**, *85* (7), 1086–1097.

(50) Wu, H.; Dong, Z.; Li, H.; Khan, M. An integrated process analytical technology (PAT) approach for pharmaceutical crystallization process understanding to ensure product quality and safety: FDA scientist's perspective. *Org. Process Res. Dev.* **2015**, *19*, 89–101.

(51) Henderson, R. K.; Jiménez-González, C.; Constable, D. J. C.; Alston, S. R.; Inglis, G. G. A.; Fisher, G.; Sherwood, J.; Binks, S. P.; Curzons, A. D. Expanding GSK's solvent selection guide – embedding sustainability into solvent selection starting at medicinal chemistry. *Green Chem.* **2011**, *13* (4), 854–862.

(52) Jolliffe, H. G.; Gerogiorgis, D. I. Process modelling, design and technoeconomic evaluation for continuous paracetamol crystallisation. *Comput. Chem. Eng.* **2018**, *118*, 224–235.

(53) Hill, A. M.; Barber, M. J.; Gotham, D. Estimated costs of production and potential prices for the WHO Essential Medicines List. *BMJ Global Health* **2018**, *3* (1), e000571.

(54) Jolliffe, H. G.; Gerogiorgis, D. I. Technoeconomic optimization of a conceptual flowsheet for continuous separation of an analgesic Active Pharmaceutical Ingredient (API). *Ind. Eng. Chem. Res.* **2017**, *56* (15), 4357–4376.